frontiers | Frontiers in Earth Science

TYPE Original Research
PUBLISHED 04 July 2024
DOI 10.3389/feart.2024.1408099

OPEN ACCESS

EDITED BY
Giovanni Martinelli,
National Institute of Geophysics and Volcanology, Italy

REVIEWED BY
Gaoxue Yang,
Chang'an University, China
Ahmed Mohamed,
Assiut University, Egypt

*CORRESPONDENCE
Shengqing Xiong,
xiongsqagrs@163.com

RECEIVED 27 March 2024
ACCEPTED 07 June 2024
PUBLISHED 04 July 2024

CITATION
Fan Z, Xiong S, Yang H, Fan Z, Li F, Ge T, He J and Jia Z (2024), Discussion of deep–seated structures as plumbing systems of hydrothermal minerals using gravity and magnetic data from the West Qinling Orogenic Belt.
Front. Earth Sci. 12:1408099.
doi: 10.3389/feart.2024.1408099

Discussion of deep–seated structures as plumbing systems of hydrothermal minerals using gravity and magnetic data from the West Qinling Orogenic Belt

Zhenyu Fan[1,2], Shengqing Xiong[1,2]*, Hai Yang[1], Zhengguo Fan[1], Fang Li[1], Tengfei Ge[1], Jingzi He[1] and Zhiye Jia[1]

[1]China Aero Geophysical Survey and Remote Sensing Center for Natural Resources, Beijing, China, [2]Key Laboratory of Airborne Geophysics and Remote Sensing Geology, Ministry of Natural Resources, Beijing, China

The West Qinling Orogenic Belt (WQOB) in central China records the tectonic evolution and deep geodynamics process associated with plate collision on the northeastern margin of the Qinghai–Tibet Plateau. The study of the deep–seated West Qinling structure is beneficial for revealing the evolution of the West Qinling crust during the continental collision orogeny, and also has significance for mineral exploration. In this study, the crustal structure and the distribution of major faults in the West Qinling Orogen are calculated by processing geophysical aeromagnetic and ground gravity data. The density and magnetic susceptibility differences between the West Qinling crust and the upper mantle are calculated by fitting, and the depth and trend of the faults related are inferred from the gravity and magnetic inversion results. Due to the overall subduction of the lower crust of the Ruoergai to the West Qinling Orogenic Belt, the structural deformation within the West Qinling is strong, and the geophysical magnetic field and gravity field are suddenly changed. It is indicated that the formation of the Diebu–Sanhe fault may have a strong correlation with the Mianlue suture zone, and their intersection may penetrate into the lower crust at a depth of about 50 km or more. The West Qinling structure represents important conduits for migrating magmatic–derived hydrothermal fluids. During the continental collision, the West Qinling major faults provided hydrothermal migration channels for ore–forming materials in different tectonic periods. Meanwhile, multiple the geological activities led to the formation of mineral deposits related to magmatic hydrothermal fluids.

KEYWORDS

west Qinling, aeromagnetic data, crustal structure, mineral deposits, migration channels

1 Introduction

The Qinling Orogenic Belt (QOB) is located between the North China Block (NCB) and South China Block (SCB), and it is interpreted to have formed by the collision between blocks (Figure 1A). Several studies have obtained the collision model of the Qinling Orogenic Belt between the North China Block and South China Block (Bader et al.,

2013a; Bader et al., 2013b; Dong et al., 2013; Li et al., 2015; Ratschbacher et al., 2006; Ratschbacher et al., 2003). The QOB was formed by the subduction and collision between the southern and northern continental blocks during the Early Paleozoic–Triassic. Since then, the Central China Orogenic Belt was overprinted by the Mesozoic to Cenozoic intracontinental orogenic events, resulting in a prominent north and south division of geology. The QOB records subduction orogeny along the Paleozoic Shangdan and Triassic Mianlue sutures, and Mesozoic intracontinental orogenesis. Investigations during the past decades have established the Mianlue suture in the southern margin of the QOB, which separates the South Qinling Block (SQB) from the SCB (Dong et al., 2022; Dong et al., 2014; Dong et al., 1999; Xu et al., 2002). The Shangdan suture is represented by a series of early Paleozoic ophiolitic melanges that include ophiolites, and subduction–related volcanic and sedimentary rocks, marking the main tectonic boundary between the North Qinling Belt (NQB) (Dong et al., 2011a; Dong et al., 2011b; Sun et al., 2022; Sun et al., 2019a; Sun et al., 2019b). Based on the comprehensive study of geology, geochemistry, geochronology and metallogeny of the Qinling Orogenic Belt and its adjacent areas, predecessors have drawn inferences and conclusions 1B) (Dong and Santosh, 2016; Dong et al., 2021). The specific viewpoints are summarized as follows. Firstly, the Qinling Orogenic Belt is a composite orogenic belt mainly formed by four accretions and collisions between discrete continental blocks, such as NCB, NQB, and SCB. There were two stages of subduction between NQB and SQB in the early Paleozoic and late Paleozoic. The Early Paleozoic orogeny was a typical ocean–continent northward subduction. The subduction and consumption of the Shangdan oceanic lithosphere during Early Devonian was succeeded by continent–continent subduction, when the SQB micro–continent subducted underneath the North Qinling Terrane (NQT) from Middle Devonian to Early Triassic. Secondly, the Triassic collisional orogeny occurred between the South Qinling Block and South China Block along the Mianlue suture. After the collision, the whole Qinling Orogenic Belt evolved into an intra–continental orogen. These multiple orogenies finally resulted in the present complex mineralization, the genetic types, spatial distribution and metallogenic epochs. During the Hercynian, sedimentary iron deposits were mainly developed in the WQOB, with relatively small tonnages and scattered distribution. During the Indosinian to Yanshanian, large and medium sized shallow medium–low temperature hydrothermal gold deposits were widely developed in the WQOB. The typical examples include the Zaozigou and Dashui gold deposit. There are still some controversies about the composition of the Qinling Orogenic Belt. For instance, the tectonic affinity of the NQT is the nucleus of the NQB and the correlation between the NQT, SQB and NCB has remained controversial (Dong and Santosh, 2016; Li et al., 2023; Wang et al., 2023). Some research results indicate that the Qinling Complex represents the high–grade metamorphic basement of the NQB and the nucleus of the NQT and is interpreted as a discrete Precambrian terrane separated from the NCB by the Kuanping suture (Dong et al., 2014; Sun et al., 2022). The NQT was originally the southern part of the NCB, and was split from the Southern NCB since the spreading of the Paleozoic Erlangping back–arc Basin or the Kuanping Proterozoic back–arc Basin (Meng and Zhang, 1999; Dong et al., 2011a; Dong et al., 2011b; Dong et al., 2008). The focus is the important role of the deep–seated structure of the West Qinling Orogenic Belt in the hydrothermal metallogenic system, and the multiple orogenic geological evolution process of the entire West Qinling orogenic region is one of the important parts of the research that cause the current geological framework (Figure 1). We make the above brief overview on the basis of the existing tectonic research results.

The West Qinling Orogenic belt is connected to the west by the Qilian Kunlun Orogenic belt, forming the southern boundary of the northeastern margin of the Qinghai–Tibet Plateau (QTP) (He et al., 2017; Yang H. Q. et al., 2022). Due to the importance of the unique geographical location of the WQOB, more studies have been carried out on the provenance and tectonic significance, tectonic evolution and tectonic significance of the ophiolite complexes and island arc rocks, and sedimentary rocks in the WQOB (Wu et al., 2014; Yang et al., 2018; Xiao et al., 2022). In the past, geophysical deep seismic reflection profiles or broadband magnetotelluric data were used to study the WQOB (Gao et al., 2014; Wang et al., 2014; Xue et al., 2019; Liu et al., 2021b). There is little research on the deep–seated crustal structure and shallow ore–forming rock masses in the WQOB based on gravity and magnetic methods. Especially after several decades of aeromagnetic surveys, the measured data now cover nearly the entire Chinese continent and part of the China Sea. The interpretation of supplementary gravity and magnetic data, as an important part of geophysics, helps to increase the understanding of the deep–seated structural system of WQOB. Combined with the results of gravity modeling, calculating the depth of the Curie point based on airborne magnetic data can provide effective information for studying deep magma chamber (Mohamed et al., 2022a). The gold deposits in the WQOB are mainly divided into orogenic, Carlin type and Carlin–like type (Liu et al., 2015a; Mao et al., 2002). Moreover, research results indicate that the West Qinling metallogenic belt has potential for mineral resources, with an estimated amount of Au resources exceeding 2000t (Weng et al., 2023). In the exploration process of metal mines, it is important to detect the tilt direction of deep buried rock masses and their edges through gravity and magnetic measurements. The aeromagnetic data is significant in mineral exploration since they are useful for the discovery of the structure (Mohamed et al., 2022b). Using the high–precision aeromagnetic data from the West Qinling, the characteristics of metalliferous deposits or ore–bearing geological bodies can be obtained by 2D or 3D forward and inversion calculations under well constrained conditions. In several ore bodies prospecting predictions, the interactive inversion technique on profile of gravity and magnetic anomalies has been successfully applied to infer the depth and attitude of deeply buried ore bodies (Fan et al., 2014; Xiong et al., 2016; Li et al., 2020).

In this contribution, based on geophysical gravity and magnetic data, we analyze the characteristics of gravity and magnetic anomalies in the research area of the West Qinling, and measure the magnetism and density of rocks and ore samples. Boundary recognition methods are used to infer the distribution of faults, and 3D gravity and magnetic inversion methods are used to understand the overall distribution of regional physical properties. Importantly, interactive inversion of gravity and magnetic anomalies is used for the key profile, with an aim to restore the deep structure of the WQOB as possible. Finally, based on the investigation of the mineral deposits, as well as the inversion calculation of ore–forming rock masses, deep faults, magnetic basement, crustal structure, we discuss the important role of the

10.3389/feart.2024.1408099

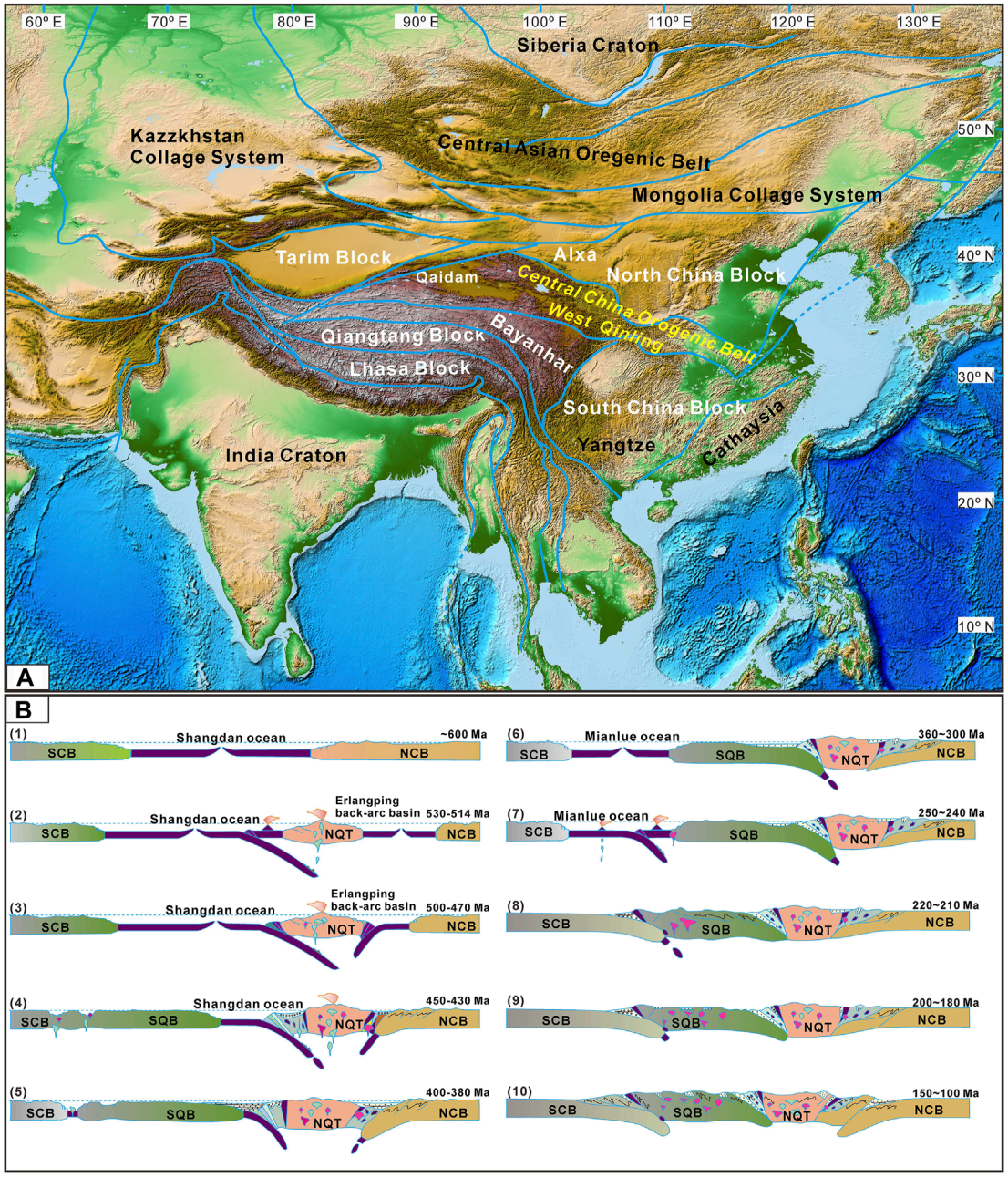

FIGURE 1
(A) Topographic simplified tectonic map showing the outline of the Central China Orogenic Belt (CCOB) where the QOB is located and related tectonic units (The DEM background was downloaded from https://www.ncei.noaa.gov, and modified from Dong et al., 2021). **(B)** Schematic cartoon for tectonic evolutionary history of the QOB (modified from Dong et al., 2021). NCB: North China Block, SCB: South China Block, SQB: South Qinling Belts, NQT: North Qinling Terrane.

WQOB as deep–seated structures of a hydrothermal minerals plumbing systems.

2 Geological setting and sampling

The location of the study area is located in the dashed line box in Figure 2. It mainly includes Ruoergai Basin, WQOB and South Qilian Orogenic Belt. The Songpan block in the northeastern QTP located at the junction of the EW and NS trending tectonic belts has affected the formation and evolution of the Chinese continent since Mesozoic and is a tectonic node in the central part of the Chinese continent. The predecessors have studied the Tangke–Hezuo deep seismic reflection profile AC, revealing the relationship between the Songpan block and the WQOB (Gao et al., 2014). However, to characterize the complicated deep–seated tectonic structure of the crust and upper mantle in the region and discuss the systems of hydrothermal minerals and mineralization processes, it is necessary

10.3389/feart.2024.1408099

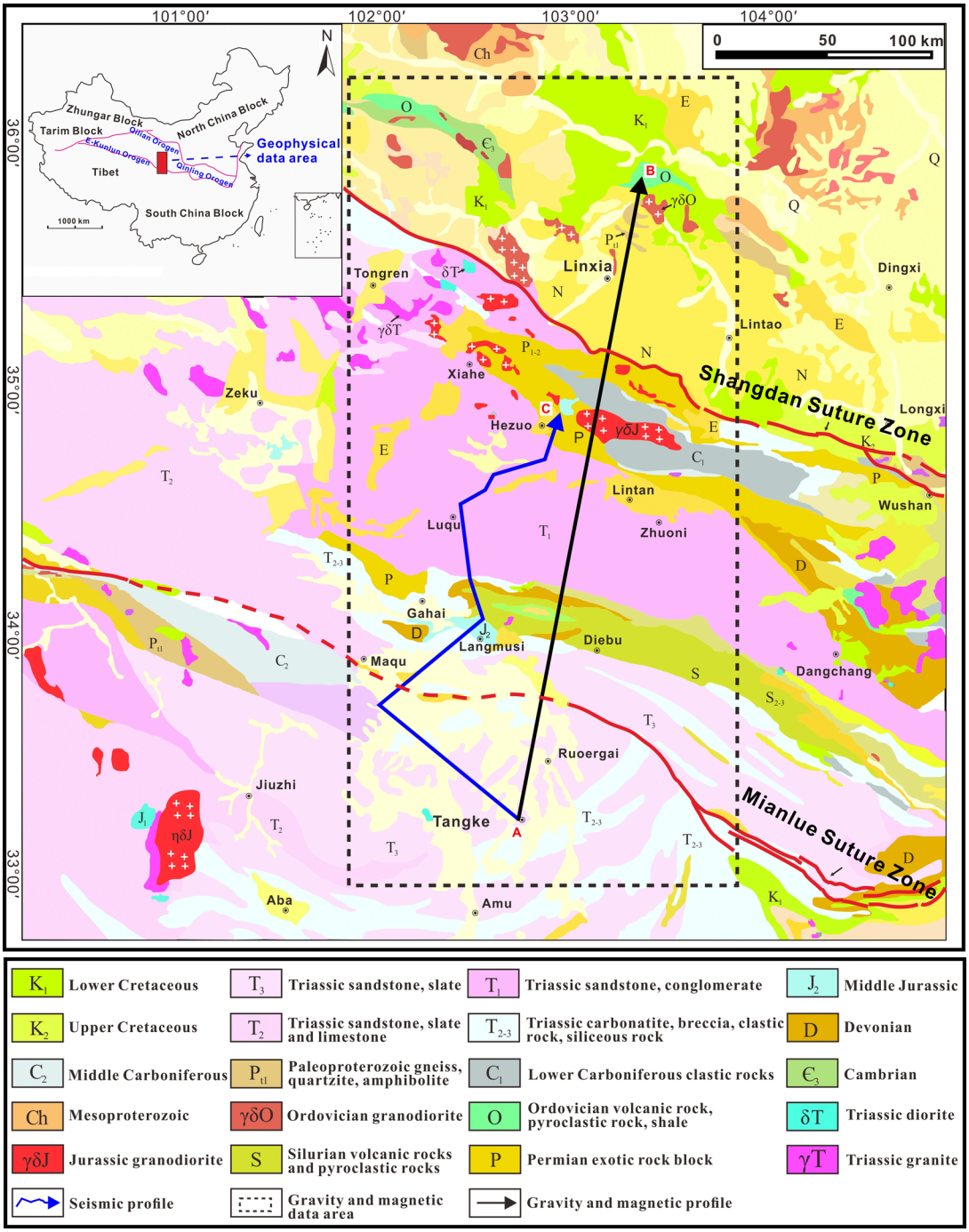

FIGURE 2
Geological map of the West Qinling research area and survey lines (modified from the geological and mineral map of Qinling metallogenic belt and adjacent areas, 1:500000). Gravity and magnetic survey lines conducted in this study. Seismic lines shown on map are sourced from Gao et al., 2014.

to conduct research based on high resolution gravity and magnetic data. In this study, we performed the first gravity and magnetic anomaly profile fitting inversion experiment across the northern margin of the Songpan block, the WQOB and the southern Qilian Orogenic Belt (profile AB in Figure 2). This profile provides us high resolution images of the lithospheric structure across the WQOB.

The Qinling Orogen located between the North China and the Yangtze cratons is a composite orogen generated by two tectonic cycles of ocean basin opening, ocean crust subduction, and continental collision. The first cycle from Ordovician to Devonian and the later from Permian to Triassic. It is generally believed that the early continental collision resulted in the Shangdan suture in the north, and the later resulted in the A'nyemaqen–Mianlue suture in the south (Dong et al., 2011b; Dong and Santosh, 2016). The area is widely covered with Triassic strata and has a large number of mineral resources, such as zinc, lead, gold, silver and copper,

etc. There are debates about the mineralization mechanism and its geodynamic control. Some research evidences indicate that the ore–forming fluids and metals may originate from post–collision metamorphism and magmatism in the WQOB. (Yu et al., 2020a; Hu et al., 2020; Wang et al., 2020; Ma et al., 2021). At present, it is generally considered that the WQOB has undergone multi–stage merging processes from the Proterozoic to late Mesozoic in the South China Block and North China Block. The magmatic activities are widely developed from the basement of the early Precambrian to the Mesozoic intracontinental orogenic tectonic evolution stage (Qiu and Deng, 2017; Qiu et al., 2021; Zhang et al., 2021). The A'nimaqen–Mianlue suture zone consists of Cambrian–Ordovician and Carboniferous–Early Permian ophiolitic blocks within a matrix of Lower to Middle Triassic flysch and represents the northeasternmost branch of the Paleo–Tethyan Ocean (Guo et al., 2007; Yan et al., 2020). In particular, several Triassic granite bodies intruded into the Paleozoic–Triassic A'nimaqen–Mianlue suture zone and are widely exposed due to erosion (Yu et al., 2020b).

Measuring the density (Table 1) and susceptibility (Table 2) of typical lithology of strata, intrusive rocks and ores in the WQOB area can reduce the multiplicity of inverse problems and effectively establish a reasonable geological–physical model. The samples for density and magnetic susceptibility in the tables were collected and measured by our research team in the field. In the process of collecting surface rock samples, we try to ensure that all types of rocks are included as much as possible. We found that the density of sedimentary rocks is relatively low, with an average variation range of 2.51–2.68 g/cm^3, and the density of metamorphic rocks varies greatly, with an average value of 2.64 g/cm^3. The density value of intrusive rock generally increases from acidic to basic, and the average density value of quartz diorite reaches 2.85 g/cm^3. Most sedimentary rocks in the area are nonmagnetic or weakly magnetic, with an average magnetic susceptibility of about 50×10^{-5} SI. However, the magnetic susceptibility of intrusive rocks generally increases gradually from acidic to ultrabasic, and the magnetic susceptibility of basic and ultrabasic intrusive rocks is the strongest, and the magnetic susceptibility of pyroxene diorite reaches 6334×10^{-5} SI. The ore is mainly magnetite and magnetite bearing Au–Cu ore, of which the magnetic susceptibility of magnetite is the highest in the region.

3 Boundary identification and results

3.1 Characteristics of gravity and magnetic anomalies

The research data are 1:50000 aeromagnetic survey results and 1:500000 ground Bouguer gravity data. We use the reduction to the pole of aeromagnetic to study and analyze the deep–seated structure of the WQOB. The West Qinling is a large area of low magnetic anomaly quiet area. The amplitude of magnetic anomaly in the Ruoergai Basin on the south side of the WQOB is relatively high, and the amplitude of magnetic anomaly in the A'nyemaqen suture zone is slightly higher than that in the south (Figure 3A). In particularly, the southern edge of the WQOB has an obvious high magnetic banded anomaly in the NW direction. The NW high magnetic anomalies are mainly in the north edge of the West Qinling to the Qilian Orogenic Belt, and there are many high and low anomaly conversion areas. The scattered cluster high magnetic anomalies are consistent with the location of volcanic and intrusive rocks exposed on the surface. The magnetic anomaly amplitude of profile AB magnetic anomaly is—48.8 nT~159.1 nT, with the highest point at the northernmost end of the survey line and the lowest value at the southern edge of the Qilian Orogenic Belt.

The QTP is the negative anomaly area with the lowest gravity anomaly value in China (Figure 3B). The northeast of the QTP is bounded by a huge gravity gradient belt. In the region, the gravity anomaly value increases gradually from southwest to northeast, and the gravity anomaly at profile AB also increases from south to north. There are obvious changes at the main faults and both sides, with the amplitude—386.2 mGal ~−253.0 mGal. These gravity anomalies are related to widely exposed magmatic and metamorphic rocks.

3.2 Boundary detection for gravity and magnetic potential field

The first vertical derivative of gravity anomalies and magnetic anomalies can enhance the gravity and magnetic effects of shallow near–surface geological bodies and suppress the influence of deep regional background field (Figures 4A, C). The first horizontal derivative of gravity anomaly and magnetic anomaly along the horizontal 45° direction focus on the shallow near–surface geological body, which has a good identification for the geological structure line perpendicular to this direction, and is also a sufficient basis for the division of secondary fault zone (Figures 4B, D). Generally, the total gradient mode of magnetic anomaly has a good correspondence with the shallow boundary (Figure 4E). The tilt derivative of magnetic anomaly and the horizontal gradient of tilt derivative of magnetic anomaly have the effect of enhancing boundary recognition (Figures 4F, G). There are still clear traces when the deep and large faults extend upward for 0.5–20 km (Figure 4H–L). Based on the above results, gravity edge detection lines reflect the boundary of density difference, while aeromagnetic edge detection lines reflect the boundary of geological body with magnetic difference. In order to better identify hidden faults, it is necessary to carry out comprehensive comparative analysis with known fault structures at different scales.

3.3 Multi–scale edge detection of gravity and magnetic fields

Through comparative experiments and practical applications, it is recognized that multi–scale edge detection method can more accurately extract model boundaries and is more suitable for structural information recognition and extraction (Hornby et al., 1999). Multi–scale edge detection applied to gravity and magnetic data is helpful to aid the interpretation of basement structure (Austin and Blenkinsop, 2008; Hackney et al., 2015). The detection results of different extension heights are superimposed, and different color line types are used to represent the boundaries of geological bodies with different depths or scales. The calculated results can also qualitatively indicate the development depth and dip characteristics of the structure. The denser the pencil of lines, the steeper the occurrence of the boundary structure development and the larger

TABLE 1 Statistical measurements of density of typical rock in West Qinling research area.

Rock type		Number of samples	Density δ (g/cm^3)	
			Range	Average
Sedimentary rock	Sandstone	435	2.35–2.82	2.62
	Carbonate rock, limestone, dolomite	388	2.44–2.82	2.68
	Mudstone	4	2.38–2.58	2.51
Metamorphic rock	Quartzite	24	2.47–2.70	2.64
Intrusive rock	Monzonitic granite	70	2.54–2.77	2.62
	Granodiorite	106	2.56–2.88	2.66
	Quartz diorite	64	2.70–3.02	**2.85**
	Diorite	43	2.60–2.95	2.76
	Serpentinite	32	2.58–2.75	2.65

Bold values emphasize that the average density or magnetic susceptibility of this type of rock is the highest.

the dip angle. On the contrary, the sparser the pencil of lines, the slower the structural dip angle changes.

The results of multi–scale edge detection calculation using gravity and magnetic data can effectively identify a series of geological faults, including deep buried faults in the structural belt (Figure 5). In which, the boundary identification results of aeromagnetic data are consistent with the Shangdan ophiolite tectonic melange belt, namely, the West Qinling fault (Figure 5A). In particularly, according to the magnetic difference, the spatial position of Diebu–Sanhe fault is consistent with the multi–scale edge detection results, and it seems to indicate that this fault has the possibility of extending to the depth. On the other hand, the boundary recognition result of gravity data calculation shows that the density difference between the two sides of the Maqu–Tazang fault is large (Figure 5B), which is consistent with the division of Mianlue tectonic melange belt recognized by geology. The results of multi–scale edge detection also show the location of other secondary faults, such as Gahai North–Guanting fault, Hezuo–Min county–Dangchang fault.

4 Inversion of gravity and magnetic data

4.1 Three–dimensional inversion of gravity and magnetic data

The three–dimensional density and magnetic susceptibility physical property distribution of the region helps to infer the deep–seated structure of the WQOB. Firstly, the gravity and magnetic data is filtered by Butterworth band–pass filter (10 km–200 km) to calculate the residual anomaly, and then the three–dimensional inversion method under the regularization constraint is adopted (Li and Oldenburg, 1998; Li and Oldenburg, 1996). According to the research purpose, the inversion depth range is determined from the surface to the underground 60 km. The mesh generation scheme is 200×400×50, the horizontal grid spacing is 1 km, and the vertical grid spacing is increased from 0.1 km to 5 km. Finally, the 3D density distribution characteristics of ~50 km (Figure 6) and the magnetic susceptibility distribution characteristics of ~30 km (Figure 7) are calculated through iterative operation.

Bouguer gravity anomaly includes regional component reflecting deep crustal information and local residual component reflecting shallow crustal information. The general trend of Bouguer gravity anomaly is a reflection of deep crustal structure. The 3D gravity inversion results indicate that the deep density of the Ruoergai Basin is relatively high, but the density at the A'nyemaqen suture zone drops suddenly, and then gradually rises again after entering the QOB. There are low density areas in local areas. The northern margin of the WQOB is low density, and then it enters the Qilian Orogenic Belt and rapidly uplifts, and there is a sharp transformation of high and low density. The 3D magnetic inversion results show that the A'nyemaqen suture zone and the southern part of the WQOB have strong ferromagnetism, while the deep part of the northern edge of the WQOB has weak ferromagnetism. The main susceptibility features of the Qilian Orogenic Belt are local superimposed blocky and needle pattern anomalies. The magnetic susceptibility under the Qilian Orogenic Belt changes sharply, and the residual magnetic susceptibility can reach 2000×10^{-5} SI.

4.2 Interactive inversion of gravity and magnetic anomalies

Here we apply an interactive inversion technique on gravity and magnetic anomalies to study the deep geological structure of the West Qinling along Tangke–linxia (profile AB in Figure 2). Interactive inversion technologies of gravity and magnetic anomalies along the undulating terrain profile is generally expressed in 2.5 D. The core process is that gravity and magnetic anomalies are

TABLE 2 Measured statistical value of typical lithological magnetic susceptibility of each stratum, intrusive rock and ore in West Qinling research area.

Stratigraphic unit	Lithology	Number of sampling sites	Number of samples	Magnetic susceptibility ($\times10^{-5}$ SI)		
				Minimum	Maximum	Average
Neogene and Paleogene	Sandstone and conglomerate	8	240	1	58	16
Cretaceous	Sandstone and conglomerate	9	270	0	61	13
	Basalt	6	180	289	5,134	**1815**
Jurassic	Andesite	2	60	57	310	137
	Basalt andesite	1	30	219	1,283	565
	Basaltic tuff	1	30	148	464	261
	Olivine basalt	2	60	1,114	6055	**3,098**
Triassic	Conglomerate, sandstone and mudstone	29	870	0	69	19
	Tuff	1	35	2152	4,317	**2938**
	Andesite	5	150	10	1,309	202
	Volcanic breccia	1	30	493	2130	**1,221**
Permian	Limestone	6	180	0	48	7
	Marble	1	30	3	45	12
	Skarn	1	30	11	55	34
Carboniferous	Hornfelized sandstone	3	90	10	5,029	**1,350**
Devonian	Sandstone	4	120	0	26	10
Silurian	Slate and schist	8	240	0	113	27
Ordovician	Limestone	1	30	0	5	1
Cambrian	Slate	1	30	11	32	20
Yanshanian intrusive rock	Granodiorite and quartz diorite	12	360	0	1,566	78
Indosinian intrusive rock	Granodiorite, granodiorite porphyry	12	360	0	422	24
	Diorite and diorite porphyrite	5	150	0	3,936	320
Caledonian intrusive rock	Diorite	3	90	0	4,961	667
	Pyroxene diorite	1	30	2518	9,143	**6334**
Mineral	Magnetite	1	35	63046	171000	**143201**
	Magnetite bearing copper ore	1	30	339	7,400	**1749**

Bold values emphasize that the average density or magnetic susceptibility of this type of rock is the highest.

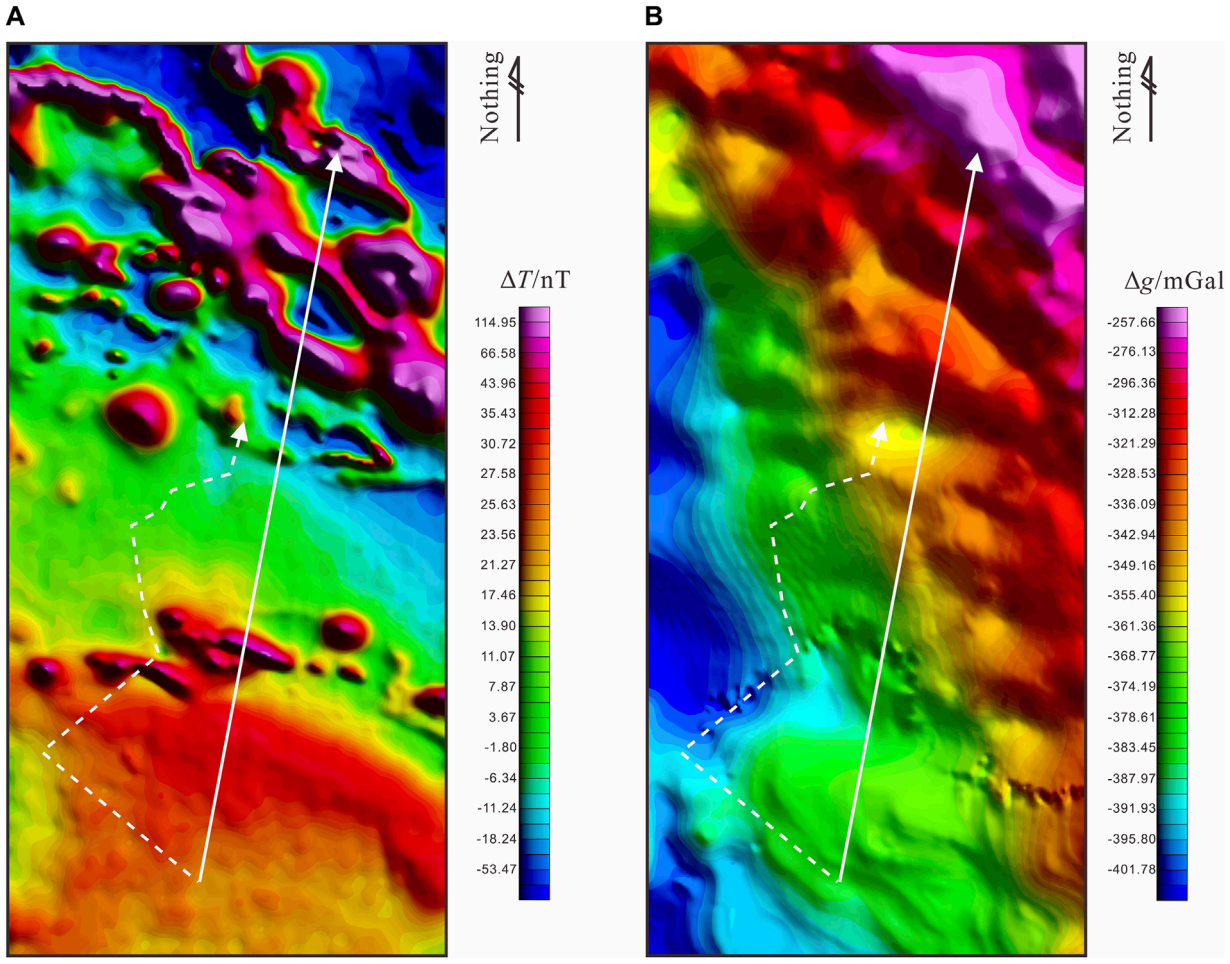

FIGURE 3
The RTP (reduction to the pole) aeromagnetic and Bouguer gravity anomalies in the West Qinling area. **(A)** The RTP aeromagnetic anomaly. **(B)** The Bouguer gravity anomaly.

calculated on the horizontal prism polygon model based on known geological structures, physical property data and semi–quantitative interpretation. After that, continue to adjust the model parameters until the calculated value of gravity and magnetic anomaly is consistent with the measured value of gravity and magnetic anomaly. Finally, we can obtain important information such as deep–seated structure, fault and metallogenic belt of the West Qinling Orogenic Belt (Figure 8).

The Curie depth in the results is calculated from aeromagnetic data. The Curie depth calculation method adopted in this article is the frequency domain high-order derivative power spectrum method (Spector and Grant, 1970), and is specifically implemented using the software GeoProbe 2.0. The depth and stratigraphic boundary of the Moho are mostly depended on the seismic reflection interface, with a depth of about 50 km. Below the Mianlue ophiolitic melange belt and the WQOB, the middle and lower crust are slightly uplifted. In addition, the overall density value of this region is relatively high. In the process of fitting the gravity and magnetic profile, the density of the upper mantle reaches 3.20 g/cm^3. The density of the lower crust in the Ruoergai Basin is 2.94 g/cm^3, and the density of the lower crust in the A'nyemaqen suture zone and the Linxia–Qinling transition zone is 2.9 g/cm^3. The maximum density of the lower crust is located in the north of the section.

The upper crust includes magnetic basement and its overlying weak magnetic strata. There are strong magnetic ore–forming rocks, intermediate–acid volcanic rocks and intermediate–basic volcanic rocks in some areas. The magnetic susceptibility of the upper crust magnetic basement at fault F4 ~ F5 is low, with a value of 20×10^{-5} SI. The magnetic susceptibility of the deep magnetic body at fault F5 ~ F6 is the lowest, with a value of 10×10^{-5} SI. The magnetic susceptibility of deep magnetic body between Tangke and fault F1 is $1{,}200\times10^{-5}$ SI. Ordovician intermediate–basic volcanic rocks exposed in the shallow part of the northernmost section, with a magnetic susceptibility value of $1{,}400\times10^{-5}$ SI. The magnetic susceptibility of medium acid granodiorite between fault F5 and F6 is 40×10^{-5} SI ~ 800×10^{-5} SI.

The initial geology model is built on the basis of cross sections (profile AB in Figure 2). Based on the range of physical properties for rocks and ores in the WQOB, we can get these physical parameters for modeling (Table 3). The parameters listed indicate that covers in the upper crustal non–magnetic or weakly magnetic. The magnetic

10.3389/feart.2024.1408099

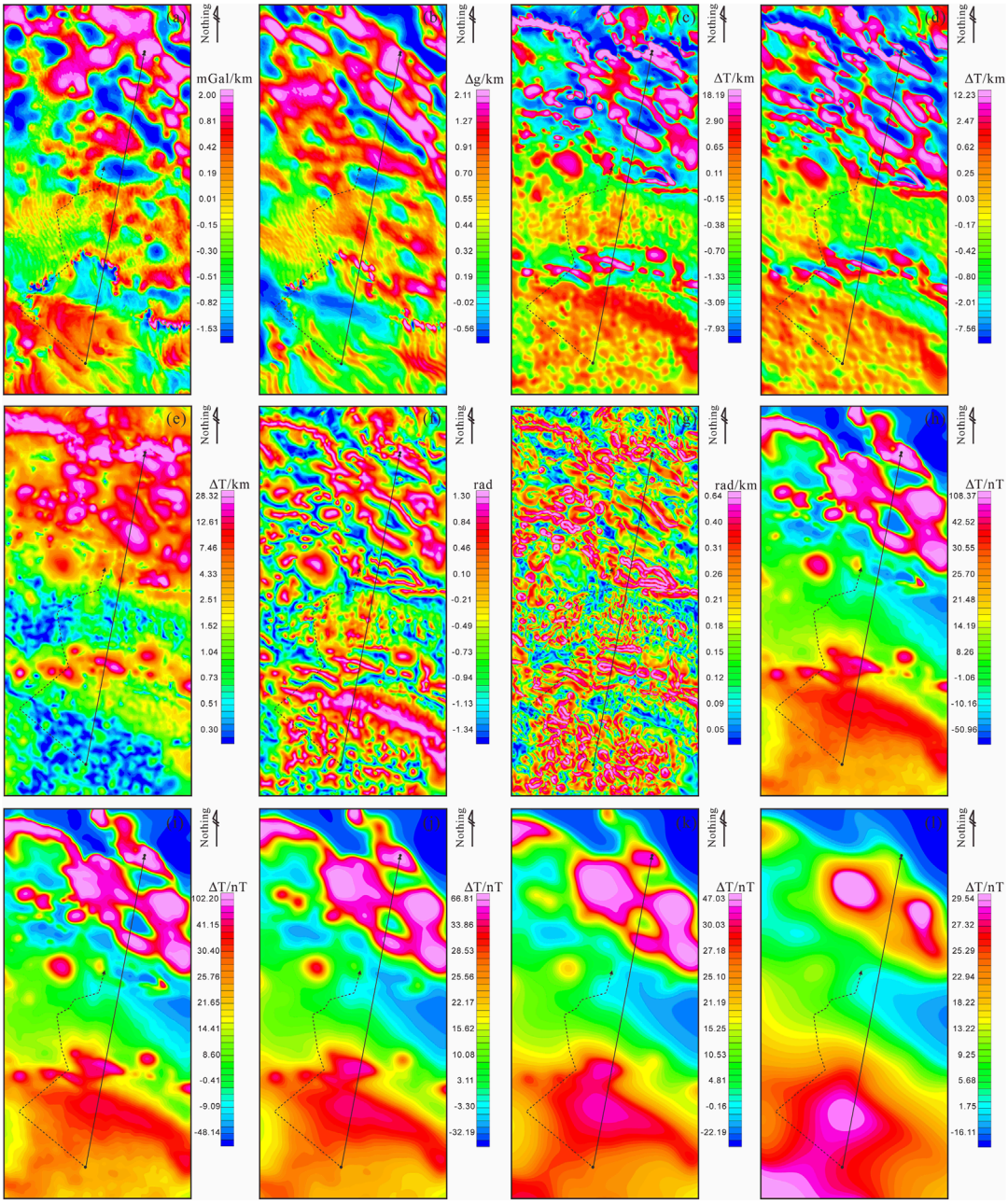

FIGURE 4
Bouguer Gravity and the RTP magnetic potential field separation. **(A)** The first vertical derivative of gravity anomaly. **(B)** The first horizontal derivative of gravity anomaly (45°). **(C)** The first vertical derivative of magnetic anomaly. **(D)** The first horizontal derivative of magnetic anomaly (45°). **(E)** The total gradient mode of magnetic anomaly. **(F)** The tilt derivative of magnetic anomaly. **(G)** The horizontal gradient of tilt derivative of magnetic anomaly **(H–L)** The RTP magnetic anomaly Upward continuation 0.5 km, 1 km, 5 km, 10 km, 20 km.

distribution of the magnetic basement in the upper crust is uneven and varies greatly. The lower crust and mantle are nonmagnetic, while the magnetic rock mass in the upper crust is the main factor causing local magnetic anomalies, especially the ferromagnetic ore–forming rock mass near the surface. The density change of the crust from top to bottom is relatively continuous, from small to large. The overall change trend of gravity anomaly is mainly caused by the horizontal direction density change of the lower crust and the fluctuation of the upper and lower crust interface. The rapid decline of gravity anomaly in local areas is caused by fault zone. In particular, the strength and the center position of magnetic anomaly significantly also depend on the shapes of iron bodies. To obtain the best results, we corrected the models of the rock mass bodies constantly, until the residual anomaly between aeromagnetic fitting curve and the measured curve is the minimum. The relative theoretical parameters indicate that the strength and the center position of gravity anomaly also depend on shapes of the models. Similarly, we can get the least residual anomaly between gravity fitting curve and the measured curve by revising the shapes of every model constantly. Consequently, when both the gravity and

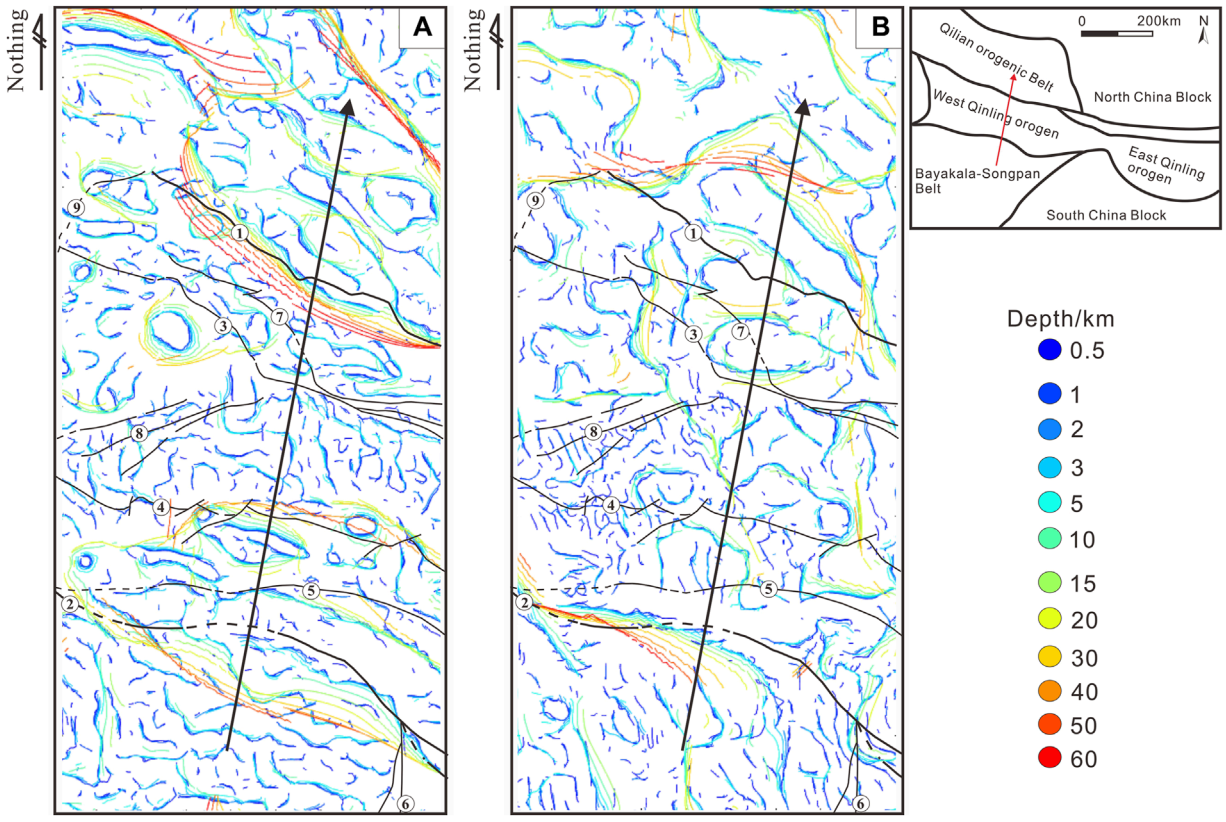

FIGURE 5
(A) Multi−scale edge detection results of aeromagnetic anomaly data. **(B)** Multi−scale edge detection results of Bouguer gravity anomaly data. Geological inferred fault: 1) Shangdan ophiolite tectonic melange belt, West Qinling (Linxia South−Wushan) fault. 2) Mianlue tectonic melange belt, Maqu−Tazang fault. 3) Hezuo−Min county−Dangchang fault. 4) Gahai North−Guanting fault. 5) Diebu−Sanhe (Bailongjiang) fault. 6) Minjiang fault. 7) Malong−Gucheng fault. 8) Ningmute−Luqu fault assemblage. 9) Longwu River fault.

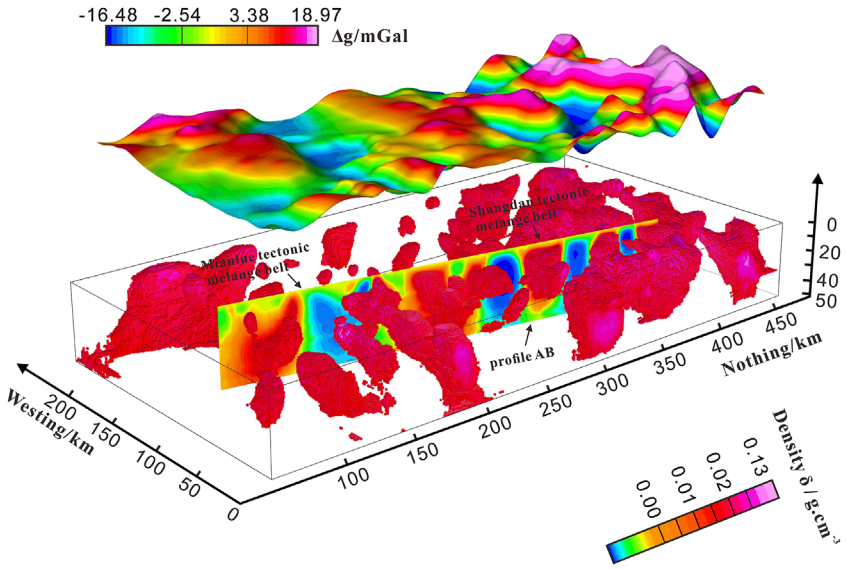

FIGURE 6
Three−dimensional structure of residual density (value >0.02 g/cm^3).

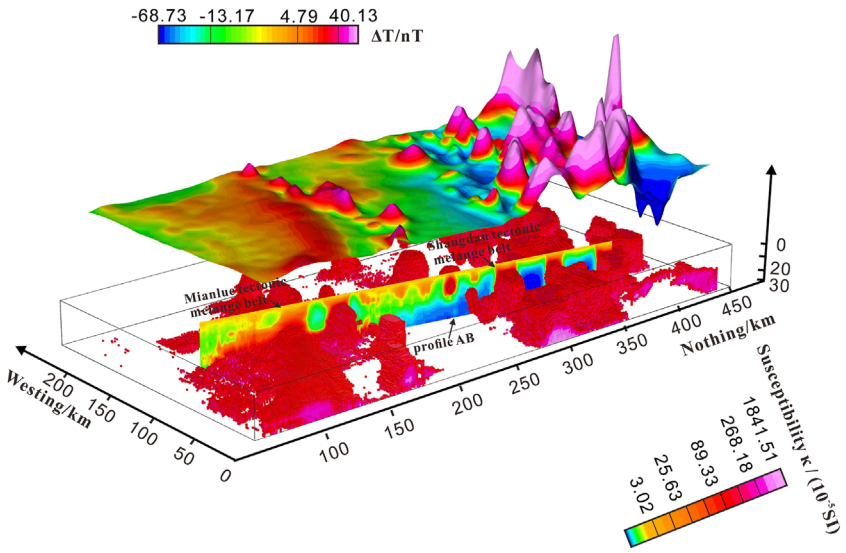

FIGURE 7
Three−dimensional structure of magnetic susceptibility (value >100×10^{-5} SI).

aeromagnetic residual anomalies are the least, we can obtain the final model for West Qinling Orogenic Belt.

5 Discussion

5.1 Characteristics of deep−seated structures in the west Qinling orogenic belt

We processed the gravity and magnetic data, and the results revealed the fine lithosphere structure of the northern margin of the Songpan block and the West Qinling Orogenic Belt, South Qilian Orogenic Belt. The research results show that the depth of Curie depth gradually rises from south to north, rising from a depth of about 40 km in the Ruoergai Basin on the north side of the profile to the shallowest of 20 km in the middle Qinling. There is a significant difference in Curie depth between the north and south sides of the Mianlue suture. According to the simulation results of density and magnetic susceptibility, the crust of the WQOB is thick, and the magnetic susceptibility in the upper crust is weak. The structure of the WQOB obtained based on gravity and magnetic data is consistent with the deep seismic reflection results (Gao et al., 2014; Wang et al., 2014; Liu W. et al., 2021), which indicates that the West Qinling underwent intensive extension after collisional orogeny. Recent studies have confirmed that the magmatism in the West Qinling is interpreted as products related to ocean subduction and continental collision, and the addition of mantle−derived magmas to the continental crust ocean subduction process played an important role in crustal growth (Kong et al., 2019; Liu H. N. et al., 2021). More importantly, the distribution of large−scale deep fault tectonic framework can be inferred through cross inversion profile fitting of gravity and magnetic anomalies, such as Mianlue structure, Shangdan structure. The inversion results indicate that the Diebu−Sanhe fault may intersect with the Mianlue suture zone in the lower crust, with a depth of about 50 km or more at the intersection, and its correlation with the Mianlue structure is worth further research.

5.2 Systems of hydrothermal minerals and mineralization processes

Based on the geophysical gravity and magnetic results of the deep−seated structure of the West Qinling, we focus on the mineralization processes related to the deposits, and describe the deep−seated tectonic hydrothermal mineral pipelining systems model of the West Qinling Orogenic belt (Figure 9A). The interactions between various interconnected magma reservoirs are widespread in West Qinling beneath the magmatic plumbing system, with multiple magmatic processes, and mineralization is likely genetically tied to magmatism (Song et al., 2023; Ma et al., 2024; Zhang et al., 2024). At present, three genetic models of Mesozoic gold mineralization have been proposed in the West Qinling Orogen (Guo et al., 2023). One model invokes a metal source from the metamorphism of crustal rocks during a regional thermal event resulting from the collision between the Yangtze and the North China cratons (Qiu et al., 2020; Yu et al., 2020b). The second model argues that the origin of gold deposits is intrusion−related and that the metals are derived from magmatic−hydrothermal fluids (Sui et al., 2020; Sui et al., 2017; Jin et al., 2017). The last model favors Carlin−like gold deposits and considers metal sources from magmatic and sedimentary rocks (Chen and Santosh, 2014; Liu et al., 2015a; Du et al., 2021b). This article takes some typical mineral deposits as the objects of analysis and discussion. The locations of these mineral deposits are distributed within the WQOB (Figure 9B). The Zaozigou and Dashui are considered Carlin−like gold deposits, and their formation is closely related to magmatic fluids. The ore−forming hydrothermal fluid of Carlin type gold deposits in the West Qinling is mainly magmatic water, with the participation of metamorphic water and atmospheric

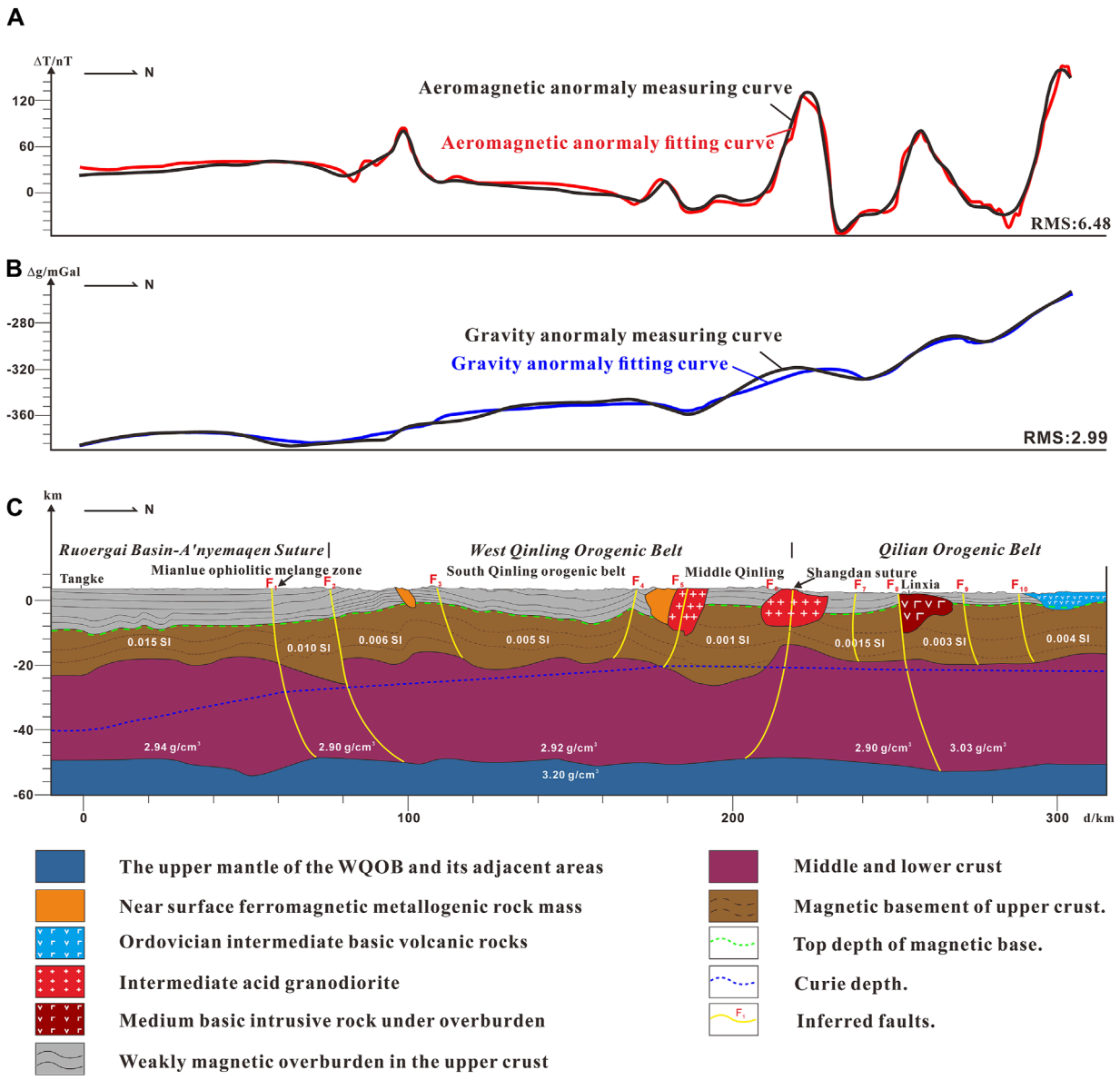

FIGURE 8
The results of interactive inversion on gravity and aeromagnetic anomalies along Tangke–Linxia (profile AB). **(A)** Fitting results of aeromagnetic anomaly curve values. **(B)** Fitting results of gravity anomaly curve values. **(C)** Inferred geological section based on inversion results.

precipitation. The Zaozigou gold deposit is associated with multiple magmatic hydrothermal activities (Du et al., 2021b; Hu et al., 2021; Hu et al., 2022), and it can be considered as a shallow–seated, distal product of a reduced intrusion–related gold system. Isotopes indicate that the ore–forming fluids are likely a mixture of magmatic fluids exsolved from a reduced magma or a mixture of such a fluid with metamorphic–derived fluids devolatized from Paleozoic sedimentary sequence underlain by the ore–hosting Triassic strata (Sui et al., 2020). Laerma is considered as a Carlin type gold deposit, which is in the background of collision Orogenic belt compression structure. The formation of the Laerma deposit is closely related to the meteoric origin fluid, and some of it is also added by magmatic water and metamorphic water (Liu et al., 2015b; Deng and Wang, 2016). Synthesis of regional geologic and geochemical data on granitic intrusions and ore deposits suggests that the Laodou is a reduced intrusion–related Au deposit, and hydrothermal fluid components were largely derived from magmas represented by the quartz diorite (Jin et al., 2017). The Dewulu has been recognized as a sediment–and magmatic–hosted sheeted vein–type reduced Au–Cu skarn deposit, which is associated with reduced felsic to intermediate intrusions emplaced during early to middle Triassic (Sui et al., 2017).

In addition, the formation process of ore deposits related to Mesozoic fluid process are briefly summarized as follows. In the initial stage of mineralization, the late Paleozoic sedimentary mineralization superimposed shallow Metamorphism and hydrothermal process. Seafloor hydrothermal eruptions led to the formation of deposits containing gold. Following Indosinian to Yanshanian hydrothermal transformation, layer–controlled

TABLE 3 Physical properties of rocks and ores on gravity and aeromagnetic inversion along Tangke–Linxia (profile AB).

Name		Density δ (g/cm^3)	Susceptibility κ (×10^{-5} SI)
Physical properties in the crust	Weakly magnetic stratigraphic	2.62–2.69	0–300
	Magnetic basement	2.62–2.70	24–1,500
	Lower crust	2.90–3.03	0
Physical properties in the mantle	Upper mantle	3.20	0
Rock mass	Ferromagnetic metallogenic rock mass	2.64–2.68	250–500
	Intermediate basic volcanic rocks	2.65	1750
	Intermediate acid granodiorite	2.65–2.70	50–1,000
	Medium basic intrusive rock	2.68	600

mineral deposits were ultimately formed. The superimposition of late magmatic intrusion or hydrothermal activation on marine volcanic sedimentary mineralization, resulting in reconstructed mineralization. In the second stage of mineralization, Mesozoic magmatic activity was associated with the widespread occurrence of iron, copper, gold, silver and other minerals in the Triassic system of West Qinling. Early to Middle Triassic marine volcanism–related deposits exhibit mineralization in marine volcanic sedimentary environments, and Late Triassic continental volcanism–related deposits are found in the western section of the Upper Triassic West Qinling. The iron, copper, gold and other mineral deposits are associated with the intrusion of acidic magma during the Triassic–Jurassic. As a result of the Indosinian movement in the Middle and Late Triassic, subduction and northward collision of the Qinling Plate occurred, leading to comprehensive uplift into landmasses. The magmatic activity persisted in localized regions until the early Yanshanian. The initial ore–forming fluid originated from magmatic water, while the later ore–forming fluid was a mixed solution of rock slurry water and atmospheric precipitation. After Triassic, intense intracontinental subduction occurred due to active intracontinental orogeny. The thermodynamic heating associated with tectonic and magmatic activity drives the convective circulation of atmospheric precipitation, causing ore–forming components in geological formations to migrate towards favorable tectonic settings for precipitation and mineralization (Lu et al., 2020; Xing et al., 2020; Du et al., 2021a; He et al., 2021; Yang X. Y. et al., 2022).

In summary, the geophysical inversion of deep–seated sturture in the West Qinling provide evidences for the opinion that metals originate from magmatic hydrothermal fluids. We support that the West Qinling structure represents important conduits for migrating magmatic–derived hydrothermal fluids. The gold, iron, and copper deposits in the study area are mainly distributed on both sides of inferred faults. The spatial distribution of gold deposits exhibits structural ore–control regularities, which are all controlled by structural systems and deep–seated fault structural belts of orders. At the end of Indosinian, with the closure of Mianlue Ocean, the tectonic setting of the West Qinling changed from oceanic subduction to continental collision. The lithosphere thermal anomaly caused by crustal thinning due to oceanic subduction is likely to provide heat source for hydrothermal activities in the WQOB. Accompanied by magmatic activity, it provides heat and material sources for mineralization. Regional magmatic activity also plays an important role in mineralization. The intrusion of granite can cause anomalies in local geothermal fields, providing a heat source for the mineralization of the intrusion–related gold deposits.

6 Conclusion

Based on the gravity and magnetic data of the West Qinling, using geophysical boundary identification and inversion technology, we draw the following conclusions.

(1) We obtained the high resolution north-south direction crossing deep–seated crustal structure of the WQOB, including density and magnetic susceptibility, and determined the distribution and extension of major faults.
(2) The research results indicate that the formation of the Diebu–Sanhe fault may have a strong correlation with the Mianlue tectonic melange structure, and intersect with the Mianlue suture zone in the lower crust, with a depth of approximately 50 km or more at the intersection.
(3) We analysised the mineralization processes in the tectonic evolution of the WQOB, and the influence of deep faults on the distribution of mineral deposits. The West Qinling structure probably represents important conduits for migrating magmatic–derived hydrothermal fluids. The West Qinling has experienced many strong tectono magmatic thermal events, and the thermal heating of the orogenic belt structure and magma has driven the convection cycle of atmospheric precipitation. In this process, the deep–seated major faults provide tectonic migration channels for metallogenic components in structures of different ages, forming mineral deposits related to hydrothermal fluids.
(4) The high-resolution magnetic and gravity research conducted is of great significance. Compared with previous research, we

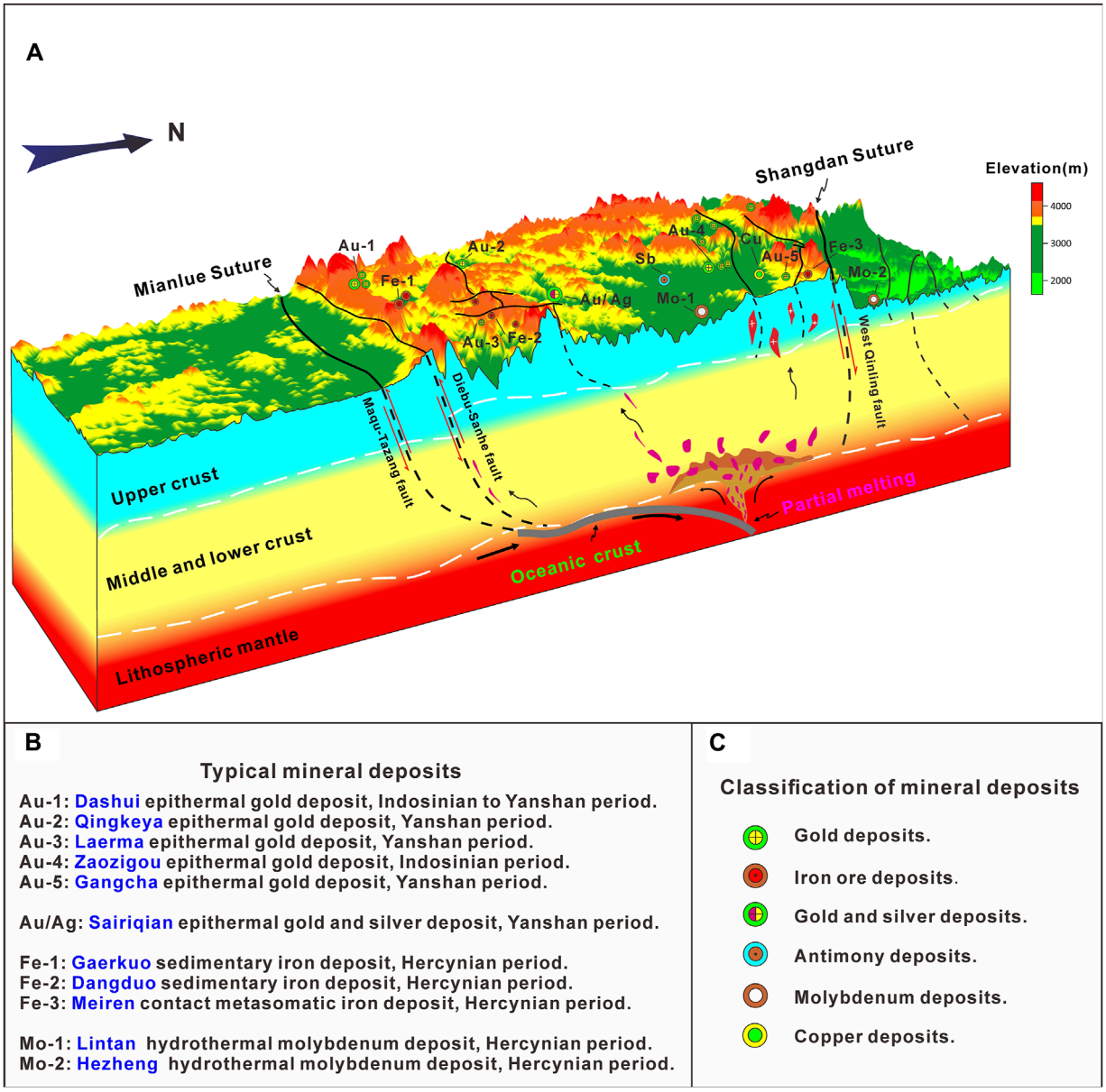

FIGURE 9
The model shows the deep–seated structures as plumbing systems of hydrothermal minerals of the West Qinling Orogenic Belt and the distribution of mineral deposits. **(A)** The deep-seated structural model of the West Qinling Orogenic Belt. **(B)** The information of typical mineral deposits discovered in this area. **(C)** The classification of mineral deposits.

have supplemented the corresponding density and magnetic susceptibility inversion results to identify some hidden deep faults. This will have a positive impact on future deep geological structure research and metal ore exploration in the region.

Data availability statement

The datasets presented in this article are not readily available because it contains confidential information held by a private company. Requests to access the datasets should be directed to the corresponding author.

Author contributions

ZF: Investigation, Writing–original draft. SX: Project administration, Supervision, Writing–review and editing. HY: Writing–review and editing. ZF: Writing–review and editing. FL: Writing–review and editing. TG: Writing–review and editing. JH: Writing–review and editing. ZJ: Writing–review and editing.

Funding

The author(s) declare that financial support was received for the research, authorship, and/or publication of this article. The authors

declare financial support was received for the research, authorship, and/or publication of this article. This study was supported by the National Natural Science Foundation of China grant (U2244220) and the China Geological Survey Project grant (DD20190551, DD20230351).

Conflict of interest

The authors declare that the research was conducted in the absence of any commercial or financial relationships that could be construed as a potential conflict of interest.

Publisher's note

All claims expressed in this article are solely those of the authors and do not necessarily represent those of their affiliated organizations, or those of the publisher, the editors and the reviewers. Any product that may be evaluated in this article, or claim that may be made by its manufacturer, is not guaranteed or endorsed by the publisher.

References

Austin, J., and Blenkinsop, T. (2008). The Cloncurry Lineament: Geophysical and geological evidence for a deep crustal structure in the eastern succession of the mount isa inlier. *Precambrian Res.* 163, 50–68. doi:10.1016/j.precamres.2007.08.012

Bader, T., Franz, L., Ratschbacher, L., de Capitani, C., Webb, A. A. G., Yang, Z., et al. (2013a). The Heart of China revisited: II early paleozoic (ultra)high-pressure and (ultra)high-temperature metamorphic qinling orogenic collage. *Tectonics* 32 (4), 922–947. doi:10.1002/tect.20056

Bader, T., Ratschbacher, L., Franz, L., Yang, Z., Hofmann, M., Linnemann, U., et al. (2013b). The heart of china revisited, I. proterozoic tectonics of the qin mountains in the core of supercontinent Rodinia: The heart of china revisited, *I. Tectonics* 32, 661–687. doi:10.1002/tect.20024

Chen, Y. J., and Santosh, M. (2014). Triassic tectonics and mineral systems in the qinling orogen, central china: triassic tectonics and mineral systems in qinling orogen, china. *Geol. J.* 49, 338–358. doi:10.1002/gj.2618

Deng, J., and Wang, Q. F. (2016). Gold mineralization in China: metallogenic provinces, deposit types and tectonic framework. *Gondwana Res.* 36, 219–274. doi:10.1016/j.gr.2015.10.003

Dong, Y. P., Liu, X. M., Neubauer, F., Zhang, G. W., Tao, N., Zhang, Y. G., et al. (2013). Timing of paleozoic amalgamation between the north china and south china blocks: evidence from detrital zircon U–Pb ages. *Tectonophysics* 586, 173–191. doi:10.1016/j.tecto.2012.11.018

Dong, Y. P., and Santosh, M. (2016). Tectonic architecture and multiple orogeny of the qinling orogenic belt, central china. *Gondwana Res.* 29, 1–40. doi:10.1016/j.gr.2015.06.009

Dong, Y. P., Sun, S. S., Santosh, M., Hui, B., Sun, J. P., Zhang, F. F., et al. (2022). Cross orogenic belts in central china: implications for the tectonic and paleogeographic evolution of the east asian continental collage. *Gondwana Res.* 109, 18–88. doi:10.1016/j.gr.2022.04.012

Dong, Y. P., Sun, S. S., Santosh, M., Zhao, J., Sun, J. P., He, D. F., et al. (2021). Central china orogenic belt and amalgamation of east asian continents. *Gondwana Res.* 100, 131–194. doi:10.1016/j.gr.2021.03.006

Dong, Y. P., Yang, Z., Liu, X. M., Zhang, X. N., He, D. F., Li, W., et al. (2014). Neoproterozoic amalgamation of the northern qinling terrain to the north china craton: constraints from geochronology and geochemistry of the kuanping ophiolite. *Precambrian Res.* 255, 77–95. doi:10.1016/j.precamres.2014.09.008

Dong, Y. P., Zhang, G. W., Hauzenberger, C., Neubauer, F., Yang, Z., and Liu, X. M. (2011a). Palaeozoic tectonics and evolutionary history of the qinling orogen: evidence from geochemistry and geochronology of ophiolite and related volcanic rocks. *Lithos* 122, 39–56. doi:10.1016/j.lithos.2010.11.011

Dong, Y. P., Zhang, G. W., Lai, S. C., Zhou, D. W., and Zhu, B. Q. (1999). An ophiolitic tectonic melange first discovered in huashan area, south margin of qinling orogenic belt, and its tectonic implications. *Sci. China Ser. D-Earth Sci.* 42, 292–302. doi:10.1007/bf02878966

Dong, Y. P., Zhang, G. W., Neubauer, F., Liu, X. M., Genser, J., and Hauzenberger, C. (2011b). Tectonic evolution of the qinling orogen, china: review and synthesis. *J. Asian Earth Sci.* 41, 213–237. doi:10.1016/j.jseaes.2011.03.002

Dong, Y. P., Zhou, M. F., Zhang, G. W., Zhou, D. W., Liu, L., and Zhang, Q. (2008). The grenvillian songshugou ophiolite in the qinling mountains, central china: implications for the tectonic evolution of the qinling orogenic belt. *J. Asian Earth Sci.* 32, 325–335. doi:10.1016/j.jseaes.2007.11.010

Du, B. S., Shen, J. F., Santosh, M., Liu, H. M., Liu, J. J., Wang, S. H., et al. (2021a). Genesis of the gangcha gold deposit, West qinling orogen, China: constraints from Rb-Sr geochronology, *in-situ* sulfur isotopes and trace element geochemistry of pyrite. *Ore Geol. Rev.* 138, 104350. doi:10.1016/j.oregeorev.2021.104350

Du, B. S., Shen, J. F., Santosh, M., Liu, H. M., Liu, J. J., Wang, Y. H., et al. (2021b). Textural, compositional and isotopic characteristics of pyrite from the zaozigou gold deposit in west qinling, china: implications for gold metallogeny. *Ore Geol. Rev.* 130, 103917. doi:10.1016/j.oregeorev.2020.103917

Fan, Z. G., Huang, X. Z., Tan, L., Yang, X., Zhang, H. R., Zhou, D. Q., et al. (2014). A study of iron deposits in the Anshan area, china based on interactive inversion technique of gravity and magnetic anomalies. *Ore Geol. Rev.* 57, 618–627. doi:10.1016/j.oregeorev.2013.09.017

Gao, R., Wang, H. Y., Zeng, L. S., Zhang, J. S., Guo, T. L., Li, Q. S., et al. (2014). The crust structures and the connection of the Songpan block and west qinling orogen revealed by the hezuo-tangke deep seismic reflection profiling. *Tectonophysics* 634, 227–236. doi:10.1016/j.tecto.2014.08.014

Guo, A. L., Zhang, G. W., Sun, Y. G., Zheng, J. K., Liu, Y., and Wang, J. Q. (2007). Geochemistry and spatial distribution of OIB and MORB in a'nyemaqen ophiolite zone: evidence of majixueshan ancient ridge-centered hotspot. *Sci. CHINA Ser. D.* 50, 197–208. doi:10.1007/s11430-007-0197-3

Guo, M. X., Liu, J. J., Zhai, D. G., De Fourestier, J., Liu, M., and Zhu, R. (2023). Tourmaline as an indicator of ore-forming processes: evidence from the laodou gold deposit, Northwest China. *Ore Geol. Rev.* 154, 105304. doi:10.1016/j.oregeorev.2023.105304

Hackney, R., Goodwin, J., Hall, L., Higgins, K., Holzrichter, N., Johnston, S., et al. (2015). Potential-field data in integrated frontier basin geophysics: successes and challenges on Australia's continental margin. *Mar. Petroleum Geol.* 59, 611–637. doi:10.1016/j.marpetgeo.2014.01.014

He, C. G., Li, J. W., Zu, B., Liu, W. J., Qiu, H. N., and Bai, X. J. (2021). Sericite 40Ar/39Ar and zircon U-Pb dating of the liziyuan gold deposit, west qinling orogen, central China: implications for ore genesis and tectonic setting. *Ore Geol. Rev.* 139, 104531. doi:10.1016/j.oregeorev.2021.104531

He, P. J., Wang, X. X., Song, C. H., Wang, Q. Q., Deng, L. Z., and Zhong, S. R. (2017). Cenozoic evolution of the western qinling Mt. Range based on thermochronologic and sedimentary records from the wudu basin, NE Tibetan plateau. *J. Asian Earth Sci.* 138, 484–494. doi:10.1016/j.jseaes.2017.02.033

Hornby, P., Boschetti, F., and Horowitz, F. G. (1999). Analysis of potential field data in the wavelet domain. *Geophys. J. Int.* 137, 175–196. doi:10.1046/j.1365-246x.1999.00788.x

Hu, Q. Q., Wang, Y. T., Mao, J. W., Liu, X. L., Chen, S. C., Wei, R., et al. (2020). Genesis of the Bafangshan-Erlihe Zn-Pb-Cu deposit in the fengxian-taibai ore cluster, west qinling, china: evidence from ore geology and ore-forming fluids. *Ore Geol. Rev.* 126, 103734. doi:10.1016/j.oregeorev.2020.103734

Hu, X. L., Ding, Z. J., Gong, Y. J., Li, K. N., and He, M. C. (2021). Ore-hosting igneous rocks in the Xiahe–Hezuo district, west qinling orogen, China, and their relationships with gold mineralization. *Ore Geol. Rev.* 133, 104127. doi:10.1016/j.oregeorev.2021.104127

Hu, X. L., Ding, Z. J., Gong, Y. J., Li, K. N., and He, M. C. (2022). Sediment-hosted disseminated gold deposits in orogenic belts: an example from the giant jiagantan gold deposit in the west qinling orogen, china. *Ore Geol. Rev.* 146, 104950. doi:10.1016/j.oregeorev.2022.104950

Jin, X. Y., Li, J. W., Hofstra, A. H., and Sui, J. X. (2017). Magmatic-hydrothermal origin of the early Triassic Laodou lode gold deposit in the Xiahe-Hezuo district, West Qinling orogen, China: implications for gold metallogeny. *Min. Deposita* 52, 883–902. doi:10.1007/s00126-016-0710-8

Kong, J. J., Niu, Y. L., Duan, M., Shao, F. L., Xiao, Y. Y., Zhang, Y., et al. (2019). The syncollisional granitoid magmatism and crust growth during the west qinling orogeny, china: insights from the Jiaochangba pluton. *Geol. J.* 54, 4014–4033. doi:10.1002/gj.3368

Li, N., Chen, Y. J., Santosh, M., and Pirajno, F. (2015). compositional polarity of triassic granitoids in the qinling orogen, china: implication for termination of the northernmost paleo-tethys. *Gondwana Res.* 27, 244–257. doi:10.1016/j.gr.2013.09.017

Li, N., Yang, L. Q., Groves, D. I., Li, H. X., Liu, X. W., Liu, J., et al. (2020). Tectonic and district to deposit-scale structural controls on the Ge'erke orogenic gold deposit within the dashui-zhongqu district, west qinling belt, china. *Ore Geol. Rev.* 120, 103436. doi:10.1016/j.oregeorev.2020.103436

Li, Y. G., and Oldenburg, D. W. (1996). 3-D inversion of magnetic data. *GEOPHYSICS* 61, 394–408. doi:10.1190/1.1443968

Li, Y. G., and Oldenburg, D. W. (1998). 3-D inversion of gravity data. *GEOPHYSICS* 63, 109–119. doi:10.1190/1.1444302

Li, Z. S., Ma, X. T., An, W., Mitchell, R. N., Li, Q. Z., Lan, Z. W., et al. (2023). Provenance transition of the mesoproterozoic–neoproterozoic xuhuai basin: constraining the accretion of the Northern qinling terrane with the north china craton. *J. Asian Earth Sci.* 251, 105675. doi:10.1016/j.jseaes.2023.105675

Liu, H. N., Li, X. W., Mo, X. X., Xu, J. F., Liu, J. J., Dong, G. C., et al. (2021a). Early Mesozoic crustal evolution in the NW segment of west qinling, china: evidence from diverse intermediate–felsic igneous rocks. *Lithos* 396–397, 106187. doi:10.1016/j.lithos.2021.106187

Liu, J. J., Dai, H. Z., Zhai, D. G., Wang, J., Wang, Y. P., Yang, L. B., et al. (2015a). Geological and geochemical characteristics and formation mechanisms of the zhaishang carlin-like type gold deposit, western qinling mountains, china. *Ore Geol. Rev.* 64, 273–298. doi:10.1016/j.oregeorev.2014.07.016

Liu, J. J., Liu, C. H., Carranza, E. J. M., Li, Y. G., Mao, Z. H., Wang, J. P., et al. (2015b). Geological characteristics and ore-forming process of the gold deposits in the western qinling region, china. *J. Asian Earth Sci.* 103, 40–69. doi:10.1016/j.jseaes.2014.11.012

Liu, W., Guo, Z., Chen, Y. S., and Zhang, A. Q. (2021b). The crustal and uppermost mantle structure of the qinling-tongbai-dabie orogenic belt from integrated geophysical observations. *Chin. J. Geophys.* 64, 3179–3193. doi:10.6038/cjg2021O0406

Lu, Y. H., Gao, P., Zhao, Z. F., and Zheng, Y. F. (2020). Whole-rock geochemical and zircon Hf–O isotopic constraints on the origin of granitoids and their mafic enclaves from the Triassic Mishuling pluton in west qinling, central china. *J. Asian Earth Sci.* 189, 104136. doi:10.1016/j.jseaes.2019.104136

Ma, J., Lü, X. B., Li, S., Fu, J. L., Mao, C., Lu, F., et al. (2021). Pyrite zonation and source of gold in the pangjiahe orogenic gold deposit, west qinling orogen, central china. *Ore Geol. Rev.* 139, 104578. doi:10.1016/j.oregeorev.2021.104578

Ma, R. L., Chen, W. T., and Tang, Y. W. (2024). magmatic and hydrothermal controls on diverse nb mineralization associated with carbonatite-alkaline complexes in the southern qinling orogenic belt, central china. *Am. Am. Mineral.* 109 (3), 574–590. doi:10.2138/am-2022-8651

Mao, J. W., Qiu, Y. M., Richard, J. G., Zhang, Z. C., Steve, G., and Ren, F. S. (2002). Geology, distribution, and classification of gold deposits in the western Qinling belt, central China. *Mineralium Deposita* 37, 352–377. doi:10.1007/s00126-001-0249-0

Meng, Q. R., and Zhang, G. W. (1999). Timing of collision of the north and south china blocks: controversy and reconciliation. *Geology* 27, 123–126. doi:10.1130/0091-7613(1999)027<0123:tocotn>2.3.co;2

Mohamed, A., Abdelrady, M., Alshehri, F., Mohammed, M. A., and Abdelrady, A. (2022b). Detection of mineralization zones using aeromagnetic data. *Appl. Sci.* 12 (18), 9078. doi:10.3390/app12189078

Mohamed, A., Al Deep, M., Abdelrahman, K., and Abdelrady, A. (2022a). Geometry of the magma chamber and curie point depth beneath hawaii island: inferences from magnetic and gravity data. *Front. earth Sci.* 10, 847984. doi:10.3389/feart.2022.847984

Qiu, K. F., and Deng, J. (2017). Petrogenesis of granitoids in the dewulu skarn copper deposit: implications for the evolution of the paleotethys ocean and mineralization in western qinling, china. *Ore Geol. Rev.* 90, 1078–1098. doi:10.1016/j.oregeorev.2016.09.027

Qiu, K. F., Yu, H. C., Deng, J., McIntire, D., Gou, Z. Y., Geng, J. Z., et al. (2020). The giant zaozigou Au-Sb deposit in West qinling, china: magmatic- or metamorphic-hydrothermal origin? *Min. Deposita* 55, 345–362. doi:10.1007/s00126-019-00937-w

Qiu, K. F., Yu, H. C., Hetherington, C., Huang, Y. Q., Yang, T., and Deng, J. (2021). Tourmaline composition and boron isotope signature as a tracer of magmatic-hydrothermal processes. *Am. Am. Mineral.* 106 (7), 1033–1044. doi:10.2138/am-2021-7495

Ratschbacher, L., Franz, L., Enkelmann, E., Jonckheere, R., Pörschke, A., Hacker, B. R., et al. (2006). "The sino-korean–yangtze suture, the huwan detachment, and the paleozoic–tertiary exhumation of (ultra)high-pressure rocks along the tongbai-xinxian-dabie mountains," in *Ultrahigh-pressure metamorphism: deep continental subduction* (Geological Society of America). Available at: https://www.researchgate.net/publication/279408693.

Ratschbacher, L., Hacker, B. R., Calvert, A., Webb, L. E., Grimmer, J. C., McWilliams, M. O., et al. (2003). Tectonics of the qinling (central china): tectonostratigraphy, geochronology, and deformation history. *Tectonophysics* 366, 1–53. doi:10.1016/s0040-1951(03)00053-2

Song, Y., Yang, L., Yang, K., Wang, B., Ma, Z., Wu, H., et al. (2023). Characteristics, geochronology, and formation conditions of W mineralization and its relationship with Au mineralization in the zhaishang gold deposit, west qinling orogen, china. *Ore Geol. Rev.* 163, 105763. doi:10.1016/j.oregeorev.2023.105763

Spector, A., and Grant, F. S. (1970). Statistical models for interpreting aeromagnetic data. *Geophysics* 35 (2), 293–302. doi:10.1190/1.1440092

Sui, J. X., Li, J. W., Hofstra, A. H., O'Brien, H., Lahaye, Y., Yan, D., et al. (2020). Genesis of the Zaozigou gold deposit, west qinling orogen, china: constraints from sulfide trace element and stable isotope geochemistry. *Ore Geol. Rev.* 122, 103477. doi:10.1016/j.oregeorev.2020.103477

Sui, J. X., Li, J. W., Wen, G., and Jin, X. Y. (2017). The dewulu reduced au-cu skarn deposit in the xiahe-hezuo district, west qinling orogen, china: implications for an intrusion-related gold system. *Ore Geol. Rev.* 80, 1230–1244. doi:10.1016/j.oregeorev.2016.09.018

Sun, S. S., Dong, Y. P., Cheng, C., He, D. F., Zhou, B., and Liu, X. M. (2022). Mesozoic intracontinental ductile shearing along the paleozoic shangdan suture in the qinling orogen: constraints from deformation fabrics and geochronology. *GSA Bull.* 134, 2649–2666. doi:10.1130/b36293.1

Sun, S. S., Dong, Y. P., Liu, X. M., He, D. F., and Cheng, C. (2019a). Fabrics, geothermometry, and geochronology of the songshugou ophiolite: insights into the tectonic evolution of the shangdan suture, qinling orogen, china. *Lithosphere* 11, 784–803. doi:10.1130/l1032.1

Sun, S. S., Dong, Y. P., Sun, Y., Cheng, C., Huang, X. X., and Liu, X. M. (2019b). Re-Os geochronology, O isotopes and mineral geochemistry of the neoproterozoic songshugou ultramafic massif in the qinling orogenic belt, china. *Gondwana Res.* 70, 71–87. doi:10.1016/j.gr.2018.12.016

Wang, H. Y., Gao, R., Li, Q. S., Li, W. H., Hou, H. S., Kuang, C. Y., et al. (2014). Deep seismic reflection profiling in the Songpan-west Qinling-Linxia basin of the Qinghai-Tibet plateau: data acquisition, data processing and preliminary interpretations. *Chin. J. Geophys.* 57, 1451–1461.

Wang, J. Y., Wang, Y. J., Lan, C. Y., and Long, X. P. (2023). Neoproterozoic tectonic evolution of north qinling orogenic belt, central china: evidence from clastic rocks. *J. Asian Earth Sci.* 251, 105672. doi:10.1016/j.jseaes.2023.105672

Wang, Y. T., Mao, J. W., Zhang, J., Wang, R. T., Chen, G. M., Hu, Q. Q., et al. (2020). Geochronological constraints on the baguamiao gold deposit, west qinling orogen, central China: implications for ore genesis and geodynamic setting. *Ore Geol. Rev.* 122, 103508. doi:10.1016/j.oregeorev.2020.103508

Weng, G. M., Liu, J. J., Carranza, E. J. M., Zhai, D. G., Zhang, F. F., Wang, Y. H., et al. (2023). Mineralogy and geochemistry of tellurides, selenides and sulfides from the zhaishang gold deposit, western qinling, china: implications for metallogenic processes. *J. Asian Earth Sci.* 244, 105536. doi:10.1016/j.jseaes.2022.105536

Wu, G. L., Meng, Q. R., Duan, L., and Li, L. (2014). Early Mesozoic structural evolution of the eastern west qinling, northwest china. *Tectonophysics* 630, 9–20. doi:10.1016/j.tecto.2014.05.008

Xiao, C. H., Chen, Z. L., Han, F. B., Wei, L. X., and Ma, L. T. (2022). Provenance and tectonic significance of lower triassic clastic sedimentary rocks of the west qinling orogenic belt, central china. *J. Asian Earth Sci.* 224, 105026. doi:10.1016/j.jseaes.2021.105026

Xing, H. Q., Li, X. W., Xu, J. F., Mo, X. X., Shan, W., Yu, H. X., et al. (2020). The genesis of felsic magmatism during the closure of the northeastern paleo-tethys ocean: evidence from the heri batholith in west qinling, china. *Gondwana Res.* 84, 38–51. doi:10.1016/j.gr.2020.02.014

Xiong, S. Q., Yang, H., Ding, Y. Y., Li, Z. K., and Li, W. (2016). Distribution of igneous rocks in China revealed by aeromagnetic data. *J. Asian Earth Sci.* 129, 231–242. doi:10.1016/j.jseaes.2016.08.016

Xu, J. F., Castillo, P. R., Li, X. H., Yu, X. Y., Zhang, B. R., and Han, Y. W. (2002). MORB-type rocks from the Paleo-Tethyan mian-lueyang northern ophiolite in the qinling mountains, central china: implications for the source of the low 206Pb/204Pb and high 143Nd/144Nd mantle component in the indian ocean. *Earth Planet. Sci. Lett.* 198, 323–337. doi:10.1016/s0012-821x(02)00536-8

Xue, S., Bai, D. H., Chen, Y., Ma, X. B., Chen, L., Li, X., et al. (2019). Contrasting crustal deformation mechanisms in the longmenshan and west qinling orogenic belts, NE Tibet, revealed by magnetotelluric data. *J. Asian Earth Sci.* 176, 120–128. doi:10.1016/j.jseaes.2019.01.039

Yan, Z., Fu, C. L., Aitchison, J. C., Buckman, S., Niu, M. L., and Cao, B. (2020). Triassic turbidites in the West qinling mountains, NW China: Part of the collisional songpan-ganzi basin or an active forearc basin? *J. Asian Earth Sci.* 194, 104366. doi:10.1016/j.jseaes.2020.104366

Yang, H. Q., Zhao, G. B., Jiang, H. B., Gu, P. Y., Wen, Z. L., and Li, Z. H. (2022a). Discussion on the metallogenic series of mineral deposits in the metallogenic belt of west qinling, china. *Northwest. Geol.* 55, 114–128.

Yang, L. M., Song, S. G., Allen, M. B., Su, L., Dong, J. L., and Wang, C. (2018). Oceanic accretionary belt in the West qinling orogen: links between the qinling and qilian orogens, china. *Gondwana Res.* 64, 137–162. doi:10.1016/j.gr.2018.06.009

Yang, X. Y., Dong, Y. P., Xiang, L. Z., Feng, Y. B., Liu, D. S., Luo, L., et al. (2022b). Two phases of cenozoic deformation in the wudu basin, west qinling (Central China): implications for outward expansion of the tibetan plateau. *J. Asian Earth Sci.* 229, 105152. doi:10.1016/j.jseaes.2022.105152

Yu, H. C., Qiu, K. F., Nassif, M. T., Geng, J. Z., Sai, S. X., Duo, D. W., et al. (2020a). Early orogenic gold mineralization event in the west qinling related to closure of the Paleo-Tethys Ocean – constraints from the ludousou gold deposit, central China. *Ore Geol. Rev.* 117, 103217. doi:10.1016/j.oregeorev.2019.103217

Yu, H. C., Qiu, K. F., Sai, S. X., McIntire, D. C., Pirajno, F., Duo, D. W., et al. (2020b). Paleo-tethys late triassic orogenic gold mineralization recorded by the Yidi'nan gold deposit, west qinling, china. *Ore Geol. Rev.* 116, 103211. doi:10.1016/j.oregeorev.2019.103211

Zhang, G. K., Li, X. W., Xu, J. F., Wang, F. Y., Bader, T., Cao, G. Y., et al. (2024). Multiple magmatic processes revealed by distinct clinopyroxene populations in the magma plumbing system: a case study from a Miocene volcano in west qinling, central china. *Am. Mineral.Am. Mineral.* 109 (3), 540–555. doi:10.2138/am-2022-8744

Zhang, L., Qiu, K. F., Hou, Z. L., Pirajno, F., Shivute, E., and Cai, Y. W. (2021). Fluid-rock reactions of the triassic Taiyangshan porphyry Cu-Mo deposit (west qinling, china) constrained by QEMSCAN and iron isotope. *Ore Geol. Rev.* 132, 104068. doi:10.1016/j.oregeorev.2021.104068